



Séminaire Laurent Schwartz

EDP et applications

Année 2013-2014


Josselin Garnier

Multiscale analysis of wave propagation in random media. Application to correlation-based imaging

Séminaire Laurent Schwartz — EDP et applications (2013-2014), Exposé n° XIII, 19 p.

<http://sisedp.cedram.org/item?id=SLSEDP_2013-2014____A13_0>

© Institut des hautes études scientifiques & Centre de mathématiques Laurent Schwartz, École polytechnique, 2013-2014.

 Cet article est mis à disposition selon les termes de la licence
CREATIVE COMMONS ATTRIBUTION – PAS DE MODIFICATION 3.0 FRANCE.
<http://creativecommons.org/licenses/by-nd/3.0/fr/>

Institut des hautes études scientifiques
Le Bois-Marie • Route de Chartres
F-91440 BURES-SUR-YVETTE
<http://www.ihes.fr/>

Centre de mathématiques Laurent Schwartz
UMR 7640 CNRS/École polytechnique
F-91128 PALAISEAU CEDEX
<http://www.math.polytechnique.fr/>

cedram

Exposé mis en ligne dans le cadre du
Centre de diffusion des revues académiques de mathématiques
<http://www.cedram.org/>

Multiscale analysis of wave propagation in random media. Application to correlation-based imaging

Josselin Garnier*

Abstract

We consider sensor array imaging with the purpose to image reflectors embedded in a medium. Array imaging consists in two steps. In the first step waves emitted by an array of sources probe the medium to be imaged and are recorded by an array of receivers. In the second step the recorded signals are processed to form an image of the medium. Array imaging in a scattering medium is limited because coherent signals recorded at the receiver array and coming from a reflector to be imaged are weak and dominated by incoherent signals coming from multiple scattering by the medium. If, however, an auxiliary passive (receiver) array can be placed between the reflector to be imaged and the scattering medium then the cross correlations of the incoherent signals on this array can also be used to image the reflector. This situation is important in particular in oil reservoir monitoring when auxiliary receivers can be implemented in wells and its study requires a multiscale analysis of wave propagation in random media. In this review we describe the results obtained in two recent papers using multiscale analysis of wave propagation in random media. In [J. Garnier and G. Papanicolaou, *Inverse Problems* 28 (2012), 075002] we show that if (i) the source array is infinite, (ii) the scattering medium is modeled by either an isotropic random medium in the paraxial regime or a randomly layered medium, and (iii) the medium between the auxiliary array and the object to be imaged is homogeneous, then imaging with cross correlations completely eliminates the effects of the random medium. It is as if we imaged with an active array, instead of a passive one, near the object. In [J. Garnier and G. Papanicolaou, *SIAM J. Imaging Sci.* 7 (2014), 1210] we analyze the resolution of the image when both the source array and the passive receiver array are finite. We show that for isotropic random media in the paraxial regime, imaging not only is not affected by the inhomogeneities but the resolution can in fact be enhanced. This is because the random medium can increase the diversity of the illumination. We also show analytically that this does not happen in a randomly layered medium, and there may be some loss of resolution in this case.

*Laboratoire de Probabilités et Modèles Aléatoires & Laboratoire Jacques-Louis Lions,
Université Paris Diderot, 75205 Paris Cedex 13, France garnier@math.univ-paris-diderot.fr

1 Introduction

In conventional active array imaging (see Figure 1, left), the sources are on an array located at $(\vec{x}_s)_{s=1}^{N_s}$, the receivers are at $(\vec{x}_r)_{r=1}^{N_r}$, and the two arrays are in the same plane. The array response matrix is given by

$$\{p(t, \vec{x}_r; \vec{x}_s), t \in \mathbb{R}, r = 1, \dots, N_r, s = 1, \dots, N_s\} \quad (1)$$

and consists of the signals recorded by the r th receiver when the s th source emits a short pulse. An image is formed by migrating the array response matrix. The Kirchhoff migration imaging function [3] at a search point \vec{y}^S in the image domain is given by

$$\mathcal{I}(\vec{y}^S) = \frac{1}{N_s N_r} \sum_{r=1}^{N_r} \sum_{s=1}^{N_s} p\left(\frac{|\vec{x}_s - \vec{y}^S| + |\vec{y}^S - \vec{x}_r|}{c_0}, \vec{x}_r; \vec{x}_s\right). \quad (2)$$

Here $|\vec{x} - \vec{y}|/c_0$ is a computed travel time between the points \vec{x} and \vec{y} , corresponding to a homogeneous medium with constant propagation speed c_0 . The images produced by Kirchhoff migration, that is, the peaks of the imaging function $\mathcal{I}(\vec{y}^S)$, can be analyzed easily if the background medium is homogeneous with propagation speed c_0 . For a point-like reflector the imaging function has the form of a peak whose radii in the different spatial directions define the resolution of the image. The range resolution is c_0/B , where B is the bandwidth of the probing pulse, and the cross range resolution is $\lambda_0 L/a$, where λ_0 is the central wavelength of the pulse, L is the distance from the array to the reflector, and a is the size of the array. These are the well-known Rayleigh resolution formulas [13]. When, however, the medium is inhomogeneous then migration may not work well because of multiple scattering by the medium. In weakly scattering media the images can be stabilized statistically by using coherent interferometry [8, 9, 5, 6], which is a special correlation-based imaging method. Statistical stability here means high signal-to-noise ratio for the imaging function. In strongly scattering media we may be able to obtain an image by using special signal processing methods [7] but often we cannot get any image at all because the coherent signals from the reflector received at the array are very weak compared to the incoherent backscatter from the scattering medium.

Let us consider the possibility of imaging with an auxiliary passive array, with sensors located at $(\vec{x}_q)_{q=1}^{N_q}$, and with the scattering medium between it and the surface source-receiver array (see Figure 1, right). This situation is important in particular in oil reservoir monitoring when auxiliary receivers can be implemented in wells [1]. The signals recorded by the auxiliary array form the data matrix

$$\{p(t, \vec{x}_q; \vec{x}_s), t \in \mathbb{R}, q = 1, \dots, N_q, s = 1, \dots, N_s\}. \quad (3)$$

Kirchhoff migration of this data matrix does not give good images, because there is no recorded coherent signal [20]. Our goal in this review paper is to show how we can use the auxiliary passive array data to get an image, and how the

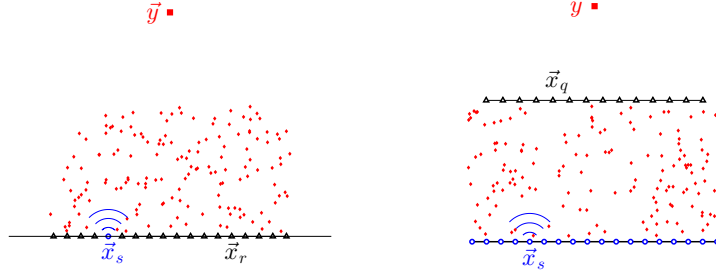


Figure 1: Sensor array imaging of a reflector located at \vec{y} through a scattering medium. Left: Conventional imaging, \vec{x}_s is a source, \vec{x}_r is a receiver. Right: Use of an auxiliary passive array for imaging through a scattering medium, \vec{x}_s is a source, \vec{x}_q is a receiver located beyond the scattering medium.

effects of the strong scattering between the passive array and the active source array can be mitigated. This will require to carry out a multiscale analysis of wave propagation in randomly scattering media.

We first give a heuristic argument based on a formal analogy with an already known situation. We may think of the strong scattering as producing signals that appear to come from spatially dispersed, statistically independent noise sources. Imaging with ambient noise sources was analyzed in [18]. By analogy with having illumination from N_s uncorrelated point sources at $(\vec{x}_s)_{s=1}^{N_s}$ emitting stationary random signals, we expect that, even in the case of active impulsive sources, the matrix of cross correlations at the auxiliary array

$$\mathcal{C}(\tau, \vec{x}_q, \vec{x}_{q'}) = \sum_{s=1}^{N_s} \int_{\mathbb{R}} p(t, \vec{x}_q; \vec{x}_s) p(t + \tau, \vec{x}_{q'}; \vec{x}_s) dt \quad (4)$$

will behave roughly as if it is the full active array response matrix of the auxiliary array, that is, the matrix of signals that would be obtained if the array consisted of N_q sources and receivers [2, 10, 17, 19]. This means that it can be used for imaging with Kirchhoff migration:

$$\mathcal{I}_C(\vec{y}^S) = \frac{1}{N_q^2} \sum_{q, q'=1}^{N_q} \mathcal{C}\left(\frac{|\vec{x}_q - \vec{y}^S| + |\vec{y}^S - \vec{x}_{q'}|}{c_0}, \vec{x}_q, \vec{x}_{q'}\right). \quad (5)$$

Motivated by this analogy with ambient noise imaging, the imaging function (5) has been the subject of our investigation in [20, 21].

In [20] we study the case when the source array has full aperture and we show analytically the striking result that the resolution of the image (5) is given by the Rayleigh resolution formulas as if the medium was homogeneous. This result is not obvious, because scattering by inhomogeneities of waves emitted

by the impulsive sources at the surface produces signals on the auxiliary passive array that are very different from those coming from spatially uncorrelated noise sources. This is especially true when addressing randomly layered media, in which scattering does not change the transverse wave vectors. Nevertheless, it has been anticipated and observed in exploration geophysics contexts [1, 27, 30] that imaging with the cross correlations of the auxiliary array is very effective and produces images that are nearly as good as in a homogeneous medium. In [20] we show this for randomly layered media in the asymptotic regime studied in detail in [15] and for isotropic random media in the paraxial regime [28, 29, 24, 11, 23].

The resolution analysis carried out in [21] in the case when the source array has partial aperture and that we reproduce in this review is based on the asymptotic expressions of the moments of the Green's function in two limiting regimes. These expressions are not new and were used previously to analyze time-reversal experiments (see [25, 26] in the random paraxial regime and [16, 14, 15] in the randomly layered regime). The enhanced resolution due to multiple scattering is known in the context of time reversal, but the imaging context considered in this review is very different. In time reversal, the recorded signals are time-reversed and re-emitted into the medium by the time-reversal array; therefore the waves propagate physically in the real medium and they can benefit from the multipathing induced by scattering. In classical imaging, the waves received at the array are backpropagated analytically or computationally in a synthetic homogeneous medium since the medium fluctuations are not known. In this case the scattering effects (in particular the random phases) cannot be removed or mitigated during the backpropagation. It turns out that the backpropagation of the cross correlation matrix of the array data in the synthetic medium can benefit from the multiply scattered wave components, provided that multiple scattering has good isotropic properties. This insight in the context of imaging is new.

In the previous paragraph we emphasized that this review is about imaging, in which backpropagation is carried out numerically in a synthetic homogeneous medium, and not about time reversal, in which backpropagation is carried out physically in the real medium. However there is a relation between the two problems when cross correlations are used for imaging. Indeed, the cross correlation (4) has an interpretation in terms of a time-reversal experiment: If we consider that the sources at $(\vec{x}_s)_{s=1}^{N_s}$ are point-like and if we use the reciprocity property of the Green's function, then the cross correlation can be written as

$$\mathcal{C}(\tau, \vec{x}_q, \vec{x}_{q'}) = \sum_{s=1}^{N_s} \int_{\mathbb{R}} p(\tau - t, \vec{x}_{q'}; \vec{x}_s) p(-t, \vec{x}_s; \vec{x}_q) dt. \quad (6)$$

This is the field observed at $\vec{x}_{q'}$ during a time-reversal experiment in the situation in which i) an original source at \vec{x}_q emits a short pulse and ii) a time-reversal array at $(\vec{x}_s)_{s=1}^{N_s}$ records the waves, time-reverses them, and re-emits them into the medium. This time-reversal interpretation of the cross correlation (4) explains why the tools used to analyze time reversal in the random paraxial

regime or in the randomly layered regime are also appropriate to analyze cross correlation imaging.

We now formulate the direct scattering problem more precisely. The space coordinates are denoted by $\vec{\mathbf{x}} = (\mathbf{x}, z) \in \mathbb{R}^2 \times \mathbb{R}$. The waves are emitted by a point source located at $\vec{\mathbf{x}}_s$ which belongs to an array of sources $(\vec{\mathbf{x}}_s)_{s=1, \dots, N_s}$ located in the plane $z = 0$. The waves are recorded by an array of receivers $(\vec{\mathbf{x}}_q)_{q=1, \dots, N_q}$ located in the plane $z = L$ (see Figure 2). The recorded signals form the data matrix (3). The scalar wave field $(t, \vec{\mathbf{x}}) \mapsto p(t, \vec{\mathbf{x}}; \vec{\mathbf{x}}_s)$ satisfies the wave equation

$$\frac{1}{c(\vec{\mathbf{x}})^2} \frac{\partial^2 p}{\partial t^2} - \Delta p = F(t, \vec{\mathbf{x}}; \vec{\mathbf{x}}_s), \quad (7)$$

where $c(\vec{\mathbf{x}})$ is the speed of propagation in the medium and the forcing term $(t, \vec{\mathbf{x}}) \mapsto F(t, \vec{\mathbf{x}}; \vec{\mathbf{x}}_s)$ models the source. It is point-like, located at $\vec{\mathbf{x}}_s = (\mathbf{x}_s, 0)$, and it emits a pulse:

$$F(t, \vec{\mathbf{x}}; \vec{\mathbf{x}}_s) = f(t)\delta(z)\delta(\mathbf{x} - \mathbf{x}_s). \quad (8)$$

We consider in this review a randomly scattering medium that occupies the section $z \in (0, L)$ and is sandwiched between two homogeneous half-spaces:

$$\frac{1}{c(\vec{\mathbf{x}})^2} = \frac{1}{c_0^2} (1 + \mu(\vec{\mathbf{x}})), \quad \vec{\mathbf{x}} \in \mathbb{R}^2 \times (0, L), \quad (9)$$

where $\mu(\vec{\mathbf{x}})$ is a zero-mean stationary random process modeling the random heterogeneities present in the medium.

We consider scattering by a reflector above the random medium placed at $\vec{\mathbf{y}} = (\mathbf{y}, L_y)$, $L_y > L$. The reflector is modeled by a local change of the speed of propagation of the form

$$\frac{1}{c(\vec{\mathbf{x}})^2} = \frac{1}{c_0^2} \left(1 + \frac{\sigma_{\text{ref}}}{|\Omega_{\text{ref}}|} \mathbf{1}_{\Omega_{\text{ref}}}(\vec{\mathbf{x}} - \vec{\mathbf{y}}) \right), \quad \vec{\mathbf{x}} \in \mathbb{R}^2 \times (L, \infty), \quad (10)$$

where Ω_{ref} is a small domain and σ_{ref} is the reflectivity of the reflector.

The recorded signals form the data matrix (3). The goal is to extract the location of the reflector from the data. The imaging function (5) that migrates the cross correlation of the recorded signals (4) is studied in [20] in the case in which the source array has full aperture, which means that it extends over the whole surface $z = 0$. In this case, both in the weakly scattering paraxial regime and in strongly scattering layered media, the correlation-based imaging function (5) produces images as if the medium between the sources and the receiver array was homogeneous and the receiver array was an active one made up of both sources and receivers. This imaging method turns out to be very efficient as it completely cancels the effect of random scattering.

In [21] the case in which the source array has finite aperture is addressed, which means that the sources do not extend over the whole surface $z = 0$. In this case it turns out that random scattering affects the resolution of the image, which is not the same with and without random scattering. The effect

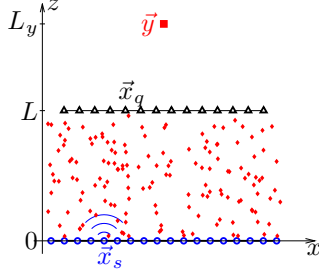


Figure 2: Sensor array imaging of a reflector through a scattering medium in the region $z \in (0, L)$. \vec{x}_s is a source, \vec{x}_q is a receiver, and \vec{y} is the reflector.

of random scattering depends on its angular properties and it may enhance or reduce the isotropy of the illumination, which in turn enhances or reduces the resolution of the imaging function (5). In [21] the weakly scattering paraxial regime, for which random scattering is good for correlation-based imaging, and the strongly scattering layered regime, for which random scattering is bad for correlation-based imaging, are analyzed. We reproduce in Section 2 the main results, and we give some more insight into the weakly scattering paraxial regime in Section 3.

2 Overview of the Results

We can give a simple explanation for why the imaging function (5) gives a good image provided that some ideal conditions are fulfilled. If the sources are point-like, generate Dirac-like pulses, and densely surround the region of interest Ω inside of which the reflector and the receiver array are, then we have (up to a multiplicative constant)

$$\hat{\mathcal{C}}(\omega, \vec{x}_q, \vec{x}_{q'}) = \int_{\partial\Omega} \hat{G}(\omega, \vec{x}_q; \vec{x}_s) \overline{\hat{G}(\omega, \vec{x}_{q'}; \vec{x}_s)} d\sigma(\vec{x}_s), \quad (11)$$

where $\hat{G}(\omega, \vec{x}_q; \vec{x}_s)$ is the time-harmonic Green's function for the wave equation (7) including the reflector:

$$\frac{\omega^2}{c(\vec{x})^2} \hat{G}(\omega, \vec{x}; \vec{x}_s) + \Delta \hat{G}(\omega, \vec{x}; \vec{x}_s) = -\delta(\vec{x} - \vec{x}_s).$$

In this review the Fourier transform of a function $f(t)$ is defined by

$$\hat{f}(\omega) = \int_{\mathbb{R}} f(t) e^{i\omega t} dt. \quad (12)$$

By the Helmholtz-Kirchhoff identity [18, 30], we find that, provided Ω is a ball with large radius,

$$\widehat{\mathcal{C}}(\omega, \vec{\mathbf{x}}_q, \vec{\mathbf{x}}_{q'}) = \frac{\omega}{c_0} \text{Im}(\widehat{G}(\omega, \vec{\mathbf{x}}_q; \vec{\mathbf{x}}_{q'})). \quad (13)$$

This shows that the cross correlation of the signals at two receivers $\vec{\mathbf{x}}_q$ and $\vec{\mathbf{x}}_{q'}$ looks like the signal recorded at $\vec{\mathbf{x}}_q$ when $\vec{\mathbf{x}}_{q'}$ is a source. Therefore, Kirchhoff Migration of the cross correlation matrix should give a good image. The use of the Helmholtz-Kirchhoff identity gives the desired result, but it obscures the important role of scattering when the source array has finite aperture. We show in this review that it is not required to have a source array that completely surrounds the region of interest to get a good image with the imaging function (5), but this result requires a deeper mathematical analysis than the often-used Helmholtz-Kirchhoff identity.

Let us first consider the situation shown in Figure 2, when the source array has full aperture and covers the surface $z = 0$, the angular illumination of the reflector is ultra-wide and the illumination cone covers the receiver array. This situation is analyzed in detail in [20]. In this case the correlation-based imaging function (5) completely cancels the effect of random scattering and the results are equivalent whatever the form of the scattering medium. The cross-range resolution of the imaging function is given by the classical Rayleigh resolution formula $\lambda_0(L_y - L)/a$, where a is the receiver array diameter. The range resolution is limited by the source bandwidth B and given by c_0/B .

The results are quite different when the source array has finite aperture and diameter b . In this case scattering turns out to play a critical role, as it may enhance or reduce the angular diversity of illumination of the reflector. This was already noticed in time reversal [12, 4, 15]: When waves emitted by a point source and recorded by an array are time-reversed and re-emitted into the medium, the time-reversed waves refocus at the original source location, and refocusing is enhanced in a scattering medium compared to a homogeneous one. This is because of the multipathing induced by scattering which enhances the refocusing cone. However this is the first time in which this result is clearly seen in an imaging context, in which the backpropagation step is carried out numerically in a fictitious homogeneous medium, and not in the physical medium. This requires the backpropagation of the cross-correlations of the recorded signals, and not the signals themselves.

We first address the case of a medium with isotropic three-dimensional weak fluctuations $\mu(\vec{\mathbf{x}})$ of the index of refraction. When the conditions for the paraxial approximation are fulfilled (see Section 3.1), backscattering can be neglected and wave propagation is governed by a Schrödinger-type equation with a random potential that has the form of a zero-mean Gaussian field whose covariance function is given by

$$\mathbb{E}[B(\mathbf{x}, z)B(\mathbf{x}', z')] = \gamma_0(\mathbf{x} - \mathbf{x}')(z \wedge z'), \quad (14)$$

with

$$\gamma_0(\mathbf{x}) = \int_{-\infty}^{\infty} \mathbb{E}[\mu(\mathbf{0}, 0)\mu(\mathbf{x}, z)]dz. \quad (15)$$

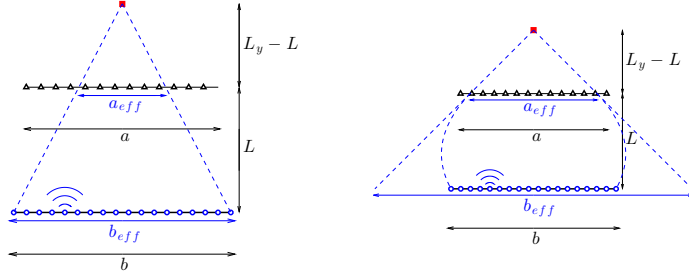


Figure 3: If the medium is homogeneous (left picture), the illumination cone is determined by the physical source array diameter $b_{\text{eff}} = b$. In the random paraxial regime (right picture), the angular diversity of the waves that illuminate the reflector is increased by scattering and the effective illumination cone is enhanced and corresponds to an effective source array diameter $b_{\text{eff}} > b$.

We show in Section 3, by using multiscale analysis, that the cone of incoherent waves that illuminates the reflector is enhanced compared to the cone of coherent waves that illuminates the reflector through a homogeneous medium (see Figure 3), and this angular cone corresponds to an effective source array diameter b_{eff} given by

$$b_{\text{eff}}^2 = b^2 + \frac{\bar{\gamma}_2 L^3}{3}, \quad (16)$$

where we have assumed that the covariance function γ_0 can be expanded as $\gamma_0(\mathbf{x}) = \gamma_0(\mathbf{0}) - \bar{\gamma}_2 |\mathbf{x}|^2 + o(|\mathbf{x}|^2)$ for $|\mathbf{x}| \ll 1$. This in turn corresponds to an effective receiver array diameter a_{eff} (defined as the intersection of the illumination cone with the receiver array) given by:

$$a_{\text{eff}} = b_{\text{eff}} \frac{L_y - L}{L_y}. \quad (17)$$

As a result, the cross-range resolution of the imaging function is given by the effective Rayleigh resolution formula $\lambda_0(L_y - L)/a_{\text{eff}}$, which exhibits a resolution enhancement since a_{eff} is larger in a random medium than in a homogeneous one. The range resolution is still given by c_0/B . The detailed analysis is in Subsection 3.4.

We next analyze the case of a medium with one-dimensional (layered) fluctuations $\mu(z)$ of the index of refraction. In this case it is known [15] that the scattering regime is characterized by strong backscattering and wave localization, with the localization length given by:

$$L_{\text{loc}} = \frac{4c_0^2}{\gamma\omega_0^2}, \quad (18)$$

where ω_0 is the noise source central frequency and

$$\gamma = \int_{-\infty}^{\infty} \mathbb{E}[\nu(z')\nu(z'+z)]dz \quad (19)$$

is the integrated covariance of the fluctuations of the index of refraction. We show in [21] that the cone of incoherent waves that illuminates the reflector is reduced compared to the cone of coherent waves that illuminates the reflector through a homogeneous medium (see Figure 4), because scattering does not change the transverse wavevector, and this angular cone corresponds to an effective source array diameter b_{eff} given approximately by

$$b_{\text{eff}}^2 = \frac{4L_y^2 L_{\text{loc}}}{L}, \quad (20)$$

where we have assumed that $b^2 \gg LL_{\text{loc}}$. This again corresponds to an effective receiver array diameter a_{eff} given by:

$$a_{\text{eff}} = b_{\text{eff}} \frac{L_y - L}{L_y}. \quad (21)$$

As a result the cross-range resolution of the imaging function is given by the effective Rayleigh resolution formula $\lambda_0(L_y - L)/a_{\text{eff}}$, which exhibits a resolution reduction since a_{eff} is smaller in a randomly layered medium than in a homogeneous medium. Furthermore, as wave scattering is strongly frequency-dependent, the effective bandwidth is reduced as well

$$B_{\text{eff}} = \frac{B}{\sqrt{1 + \frac{B^2 L}{4\omega_0^2 L_{\text{loc}}}}}, \quad (22)$$

and the range resolution is given by c_0/B_{eff} .

The comparative analysis of the random paraxial regime and the randomly layered regime clearly exhibits the role of scattering in correlation-based imaging for configurations with auxiliary receiver arrays. With a source array with full aperture, scattering plays no role as the illumination of the reflector is ultra-wide whatever the scattering regime. When the source array is limited, if scattering is isotropic, then it enhances the angular diversity of the illumination of the reflector and the resolution of the correlation-based imaging function. If it is anisotropic, then it reduces the angular diversity of the illumination of the reflector and the resolution of the correlation-based imaging function.

We note, however, that a large physical source array and/or broadband sources are necessary to ensure the statistical stability of the imaging function. This has been addressed in detail in different contexts in [6, 22].

3 Analysis in the Paraxial Regime

3.1 The Paraxial Scaling Regime

In this section we analyze a scaling regime in which scattering is isotropic and weak, which allows us to use the random paraxial wave model to describe wave

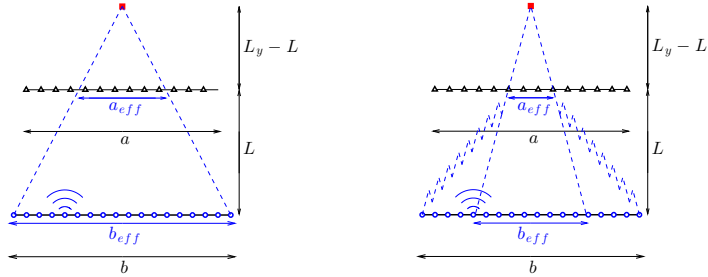


Figure 4: If the medium is homogeneous (left picture), the illumination cone is determined by the physical source array diameter $b_{\text{eff}} = b$. If the medium is randomly layered (right picture), the angular diversity of the waves that illuminate the reflector is reduced by scattering (only the waves with wavevectors close to the vertical direction can reach the reflector after multiple scattering events that conserve the wavevectors in the layered case) and the effective illumination cone is reduced and corresponds to an effective source array diameter $b_{\text{eff}} < b$.

propagation in the scattering region. In this approximation, backscattering is negligible but there is significant lateral scattering as the wave advances. Even though scattering is weak, its effects accumulate over long propagation distances and it can be a limiting factor in imaging and communications if not mitigated in some way. Wave propagation in random media in the paraxial regime has been used extensively in underwater sound propagation as well as in the microwave and optical contexts in the atmosphere [29, 28]. We formulate the regime of paraxial wave propagation in random media with a scaling of parameters that allows detailed and effective mathematical analysis [23]. It is described as follows.

1) We assume that the correlation length l_c of the medium is much smaller than the typical propagation distance L . We denote by ε^2 the ratio between the correlation length and the typical propagation distance:

$$\frac{l_c}{L} \sim \varepsilon^2. \quad (23)$$

2) We assume that the transverse width R_0 of the source (array) and the correlation length of the medium l_c are of the same order. This means that the ratio R_0/L is of order ε^2 . This scaling is motivated by the fact that, in this regime, there is a non-trivial interaction between the fluctuations of the medium and the wave.

3) We assume that the typical wavelength λ is much smaller than the propagation distance L , more precisely, we assume that the ratio λ/L is of order ε^4 :

$$\frac{\lambda}{L} \sim \varepsilon^4. \quad (24)$$

This high-frequency scaling $\lambda \ll R_0 \ll L$ is the classical paraxial regime in which the beam generated by the source propagates along a privileged direction and spreads out by diffractive effects, which are of order one provided $L\lambda/R_0^2$ is of order one.

4) We assume that the typical amplitude of the random fluctuations of the medium is small. More precisely, we assume that the relative amplitude of the fluctuations is of order ε^3 . This scaling has been chosen so as to obtain an effective regime of order one when ε goes to zero. That is, if the magnitude of the fluctuations is smaller than ε^3 , then the wave would propagate as if the medium was homogeneous, while if the order of magnitude is larger, then the wave would not be able to penetrate the random medium. The scaling that we consider here corresponds to the physically most interesting situation where random effects play a significant role, quantifiable within the paraxial regime.

3.2 The Random Paraxial Wave Equation

We consider the time-harmonic form of the scalar wave equation

$$(\partial_z^2 + \Delta_\perp)\widehat{p} + \frac{\omega^2}{c_0^2}(1 + \mu(\mathbf{x}, z))\widehat{p} = 0. \quad (25)$$

Here μ is a random process that models the three-dimensional spatial fluctuations of the medium properties. It is assumed to be a zero-mean and stationary process with mixing properties in the z -direction. In the high-frequency regime described above,

$$\omega \rightarrow \frac{\omega}{\varepsilon^4}, \quad \mu(\mathbf{x}, z) \rightarrow \varepsilon^3 \mu\left(\frac{\mathbf{x}}{\varepsilon^2}, \frac{z}{\varepsilon^2}\right), \quad (26)$$

the rescaled function $\widehat{\phi}^\varepsilon$ defined by

$$\widehat{p}^\varepsilon(\omega, \mathbf{x}, z) = \exp\left(i\frac{\omega}{\varepsilon^4}z\right)\widehat{\phi}^\varepsilon\left(\frac{\omega}{\varepsilon^4}, \frac{\mathbf{x}}{\varepsilon^2}, z\right) \quad (27)$$

satisfies

$$\varepsilon^4 \partial_z^2 \widehat{\phi}^\varepsilon + \left(2i\frac{\omega}{c_0}\partial_z \widehat{\phi}^\varepsilon + \Delta_\perp \widehat{\phi}^\varepsilon + \frac{\omega^2}{\varepsilon c_0^2} \mu\left(\frac{\mathbf{x}}{\varepsilon^2}, \frac{z}{\varepsilon^2}\right) \widehat{\phi}^\varepsilon\right) = 0. \quad (28)$$

The ansatz (27) corresponds to an up-going plane wave with a slowly varying envelope. In the regime $\varepsilon \ll 1$, it has been shown in [23] that the forward-scattering approximation and the white-noise approximation are both valid, which means that the second-order derivative in z in (28) can be neglected and the random potential $\frac{1}{\varepsilon} \mu\left(\frac{\mathbf{x}}{\varepsilon^2}, \frac{z}{\varepsilon^2}\right)$ can be replaced by a Gaussian field that is white noise in the z -direction. The mathematical statement is that the random function $\widehat{\phi}^\varepsilon(\omega, \mathbf{x}, z)$ converges in distribution to the solution $\widehat{\phi}(\omega, \mathbf{x}, z)$ of the Itô-Schrödinger equation

$$2i\frac{\omega}{c_0}d\widehat{\phi}(\omega, \mathbf{x}, z) + \Delta_\perp \widehat{\phi}(\omega, \mathbf{x}, z)dz + \frac{\omega^2}{c_0^2} \widehat{\phi}(\omega, \mathbf{x}, z) \circ dB(\mathbf{x}, z) = 0, \quad (29)$$

where $B(\mathbf{x}, z)$ is a Brownian field, that is a Gaussian process with mean zero and covariance function (14). Here the \circ stands for the Stratonovich stochastic integral [23]. We introduce the fundamental solution $\widehat{G}(\omega, (\mathbf{x}, z), (\mathbf{x}_0, z_0))$, which is defined as the solution of the equation in (\mathbf{x}, z) (for $z > z_0$):

$$2i \frac{\omega}{c_0} d\widehat{G} + \Delta_{\perp} \widehat{G} dz + \frac{\omega^2}{c_0^2} \widehat{G} \circ dB(\mathbf{x}, z) = 0, \quad (30)$$

starting from $\widehat{G}(\omega, (\mathbf{x}, z = z_0), (\mathbf{x}_0, z_0)) = \delta(\mathbf{x} - \mathbf{x}_0)$. In a homogeneous medium ($B \equiv 0$) the fundamental solution is (for $z > z_0$)

$$\widehat{G}_0(\omega, (\mathbf{x}, z), (\mathbf{x}_0, z_0)) = \frac{\omega}{2i\pi c_0(z - z_0)} \exp\left(i \frac{\omega |\mathbf{x} - \mathbf{x}_0|^2}{2c_0(z - z_0)}\right). \quad (31)$$

In a random medium, the first two moments of the random fundamental solution have the following expressions.

Proposition 3.1 *The first order-moment of the random fundamental solution exhibits frequency-dependent damping:*

$$\mathbb{E}[\widehat{G}(\omega, (\mathbf{x}, z), (\mathbf{x}_0, z_0))] = \widehat{G}_0(\omega, (\mathbf{x}, z), (\mathbf{x}_0, z_0)) \exp\left(-\frac{\gamma_0(\mathbf{0})\omega^2|z - z_0|}{8c_0^2}\right), \quad (32)$$

where γ_0 is given by (15).

The second order-moment of the random fundamental solution exhibits frequency-dependent spatial decorrelation:

$$\begin{aligned} \mathbb{E}[\widehat{G}(\omega, (\mathbf{x}, z), (\mathbf{x}_0, z_0)) \overline{\widehat{G}(\omega, (\mathbf{x}', z), (\mathbf{x}_0, z_0))}] \\ = \widehat{G}_0(\omega, (\mathbf{x}, z), (\mathbf{x}_0, z_0)) \overline{\widehat{G}_0(\omega, (\mathbf{x}', z), (\mathbf{x}_0, z_0))} \\ \times \exp\left(-\frac{\gamma_2(\mathbf{x} - \mathbf{x}')\omega^2|z - z_0|}{4c_0^2}\right), \end{aligned} \quad (33)$$

where

$$\gamma_2(\mathbf{x}) = \int_0^1 (\gamma_0(\mathbf{0}) - \gamma_0(\mathbf{x}s)) ds, \quad (34)$$

with γ_0 given by (15).

These are classical results (see [24, Chapter 20] or [23]) once the random paraxial equation has been proved to be correct, as is the case here. The result (32) on the first-order moment shows that any coherent wave imaging method cannot give good images if the range is larger than the scattering mean free path $l_{\text{sca}} = 8c_0^2/(\gamma_0(\mathbf{0})\omega^2)$, because the coherent wave components are then exponentially damped. This is the situation we have in mind, and this is the situation in which imaging by migration of cross correlations turns out to be efficient. The result (33) on the second-order moment is used in the next subsection to analyze the cross correlation of the recorded signals in a quantitative way. Note that $\gamma_2(\mathbf{0}) = 0$, which implies that the fields recorded at two nearby points are correlated.

3.3 The Cross Correlation of the Recorded Field

We consider again the situation described in Figure 2. In the random paraxial scaling regime described above, the scalar field $p^\varepsilon(t, \vec{\mathbf{x}}; \vec{\mathbf{x}}_s)$ corresponding to the emission from an element $\vec{\mathbf{x}}_s = (\varepsilon^2 \mathbf{x}_s, 0)$ of the surface source array is solution of

$$\frac{1}{c^\varepsilon(\vec{\mathbf{x}})^2} \frac{\partial^2 p^\varepsilon}{\partial t^2} - \Delta p^\varepsilon = F^\varepsilon(t, \vec{\mathbf{x}}; \vec{\mathbf{x}}_s), \quad (35)$$

where

– the source term is $F^\varepsilon(t, \vec{\mathbf{x}}; \vec{\mathbf{x}}_s) = f^\varepsilon(t) \delta(z) \delta(\mathbf{x} - \varepsilon^2 \mathbf{x}_s)$, with $\vec{\mathbf{x}} = (\mathbf{x}, z)$, the pulse is of the form

$$f^\varepsilon(t) = f\left(\frac{t}{\varepsilon^4}\right), \quad (36)$$

where the support of the Fourier transform of f is bounded away from zero and of rapid decay at infinity, with central frequency ω_0 and bandwidth B ,

– the medium is random in the region $z \in (0, L)$:

$$\frac{1}{c^\varepsilon(\vec{\mathbf{x}})^2} = \frac{1}{c_0^2} \left(1 + \varepsilon^3 \mu\left(\frac{\mathbf{x}}{\varepsilon^2}, \frac{z}{\varepsilon^2}\right)\right), \quad \vec{\mathbf{x}} \in \mathbb{R}^2 \times (0, L), \quad (37)$$

and homogeneous with background velocity c_0 in the two half-spaces $z \in (-\infty, 0)$ and $z \in (L, \infty)$, except for the reflector as described by (10).

We consider the cross correlation of the signals recorded at the receiver array $(\vec{\mathbf{x}}_q)_{q=1}^{N_q}$, $\vec{\mathbf{x}}_q = (\varepsilon^2 \mathbf{x}_q, L)$, defined by:

$$\mathcal{C}^\varepsilon(\tau, \vec{\mathbf{x}}_q, \vec{\mathbf{x}}_{q'}) = \sum_{s=1}^{N_s} \int_{\mathbb{R}} p^\varepsilon(t, \vec{\mathbf{x}}_q; \vec{\mathbf{x}}_s) p^\varepsilon(t + \tau, \vec{\mathbf{x}}_{q'}; \vec{\mathbf{x}}_s) dt. \quad (38)$$

Using the Born approximation for the point reflector at $\vec{\mathbf{y}}$ in the homogeneous medium above the auxiliary receiver array, and the continuum approximation (for any smooth test function ϕ)

$$\frac{1}{N_s} \sum_{s=1}^{N_s} \phi(\mathbf{x}_s) \simeq \frac{1}{\pi b^2} \int_{\mathbb{R}^2} \phi(\mathbf{y}_s) d\mathbf{y}_s,$$

for some $b > 0$, we obtain the following proposition proved in [20].

Proposition 3.2 *In the random paraxial wave regime $\varepsilon \rightarrow 0$, when there is a point reflector at $\vec{\mathbf{y}} = (\varepsilon^2 \mathbf{y}, L_y)$ and when the source array covers the whole surface $z = 0$, then the cross correlation of the recorded signals at the receiver array satisfies*

$$\begin{aligned} \varepsilon^4 \mathcal{C}^\varepsilon\left(\frac{2L_y - 2L}{c_0} + \varepsilon^4 s, \vec{\mathbf{x}}_q, \vec{\mathbf{x}}_{q'}\right) &\xrightarrow{\varepsilon \rightarrow 0} -\frac{\sigma_{\text{ref}}}{64\pi^4 c_0 (L_y - L)^2 b^2} \int_{\mathbb{R}} i\omega |\widehat{f}(\omega)|^2 \\ &\times \exp\left(-i\omega\left(s - \frac{1}{2c_0} \frac{|\mathbf{y} - \mathbf{x}_q|^2 + |\mathbf{y} - \mathbf{x}_{q'}|^2}{L_y - L}\right)\right) d\omega, \end{aligned} \quad (39)$$

in probability.

The convergence in probability of the cross correlation comes from the self-averaging property of the product of two Green's functions when integrated over frequency, which is the case here because the bandwidth of the source (of order ε^{-4}) is much larger than the frequency coherence radius of the Green's function (of order ε^{-2}). The same mechanism ensures the statistical stability of the refocused wave during a time-reversal experiment, meaning that the focal spot of the refocused wave depends on the statistical properties of the random medium, but not on the particular realization.

This proposition shows that

– the cross correlation $\tau \rightarrow \mathcal{C}^\varepsilon(\tau, \vec{\mathbf{x}}_q, \vec{\mathbf{x}}_{q'})$ has a peak at time lag τ equal to

$$\tau_{\mathbf{x}_q, \mathbf{x}_{q'}} = \frac{2L_y - 2L}{c_0} + \frac{\varepsilon^4}{2c_0} \frac{|\mathbf{y} - \mathbf{x}_q|^2 + |\mathbf{y} - \mathbf{x}_{q'}|^2}{L_y - L}, \quad (40)$$

since

$$\varepsilon^4 \mathcal{C}^\varepsilon(\tau_{\mathbf{x}_q, \mathbf{x}_{q'}} + \varepsilon^4 s, \vec{\mathbf{x}}_q, \vec{\mathbf{x}}_{q'}) \xrightarrow{\varepsilon \rightarrow 0} -\frac{\sigma_{\text{ref}}}{64\pi^4 c_0 (L_y - L)^2 b^2} \int_{\mathbb{R}} i\omega |\hat{f}(\omega)|^2 e^{-i\omega s} d\omega \quad (41)$$

has a peak centered at $s = 0$. The time lag $\tau_{\mathbf{x}_q, \mathbf{x}_{q'}}$ is the sum of travel times from $\vec{\mathbf{x}}_q$ to $\vec{\mathbf{y}}$ and from $\vec{\mathbf{y}}$ to $\vec{\mathbf{x}}_{q'}$ in the paraxial approximation:

$$\begin{aligned} & \frac{|\vec{\mathbf{x}}_q - \vec{\mathbf{y}}|}{c_0} + \frac{|\vec{\mathbf{y}} - \vec{\mathbf{x}}_{q'}|}{c_0} \\ &= \frac{1}{c_0} \sqrt{(L_y - L)^2 + \varepsilon^4 |\mathbf{y} - \mathbf{x}_q|^2} + \frac{1}{c_0} \sqrt{(L_y - L)^2 + \varepsilon^4 |\mathbf{y} - \mathbf{x}_{q'}|^2} \\ &= \frac{2L_y - 2L}{c_0} + \frac{\varepsilon^4}{2c_0} \frac{|\mathbf{y} - \mathbf{x}_q|^2 + |\mathbf{y} - \mathbf{x}_{q'}|^2}{L_y - L} + O(\varepsilon^8) \\ &= \tau_{\mathbf{x}_q, \mathbf{x}_{q'}} + O(\varepsilon^8). \end{aligned} \quad (42)$$

– the effect of the random medium has completely disappeared.

The conclusion is that Kirchhoff migration with cross correlations of the receiver array produces images as if the medium was homogeneous and the receiver array was active.

When the source array has a finite aperture, with the source array diameter equal to $\varepsilon^2 b$, then an important quantity is the effective source array diameter $\varepsilon^2 b_{\text{eff}}$ defined by (16). The effective source array diameter can be interpreted as the one seen from the receiver array through the random medium. It is increased by wave scattering in the random medium. As we see in the next section, this increase in turn enhances the resolution of the imaging function.

More precisely the following proposition proved in [21] shows that only the receivers that are within the cone determined by the effective source array diameter contribute to the cross correlation. As a result, the cross correlation is the same as in the case of a source array with full aperture provided that the effective array diameter is larger than a certain threshold value. In the homogeneous case, this requires that the source array diameter must be larger than the threshold value. In the random medium, the source array does not need to

be large, only the effective source array diameter needs to be larger than the threshold value, which can be achieved because of the second term in (16) which is due to scattering.

Proposition 3.3 *We consider the random paraxial wave regime $\varepsilon \rightarrow 0$, when there is a point reflector at $\vec{\mathbf{y}} = (\varepsilon^2 \mathbf{y}, L_y)$ and when the source array covers a domain of radius $\varepsilon^2 b$ at the surface $z = 0$. If the effective source array diameter is large enough in the sense that the effective Fresnel number $\frac{b_{\text{eff}}^2}{\lambda_0 L} > \frac{L_y}{L_y - L}$, where $\lambda_0 = 2\pi c_0 / \omega_0$ is the carrier wavelength, then the cross correlation of the recorded signals at the receiver array satisfies*

$$\varepsilon^4 C^\varepsilon \left(\frac{2L_y - 2L}{c_0} + \varepsilon^4 s, \vec{\mathbf{x}}_q, \vec{\mathbf{x}}_{q'} \right) \xrightarrow{\varepsilon \rightarrow 0} - \frac{\sigma_{\text{ref}}}{64\pi^4 c_0 (L_y - L)^2 b_{\text{eff}}^2} \int_{\mathbb{R}} i\omega |\hat{f}(\omega)|^2 \psi_{\text{eff}}(\mathbf{x}_q, \mathbf{y}) \times \exp \left(-i\omega \left(s - \frac{1}{2c_0} \frac{|\mathbf{y} - \mathbf{x}_q|^2 + |\mathbf{y} - \mathbf{x}_{q'}|^2}{L_y - L} \right) \right) d\omega, \quad (43)$$

in probability, where

$$\psi_{\text{eff}}(\mathbf{x}_q, \mathbf{y}) = \exp \left(- \frac{|\mathbf{x}_q - \mathbf{y}L/L_y|^2}{a_{\text{eff}}^2} \right), \quad (44)$$

with a_{eff} and b_{eff} given by (16-17).

In order to get an explicit closed-form expression for the effective truncation function ψ_{eff} , we have assumed that the source array $(\vec{\mathbf{x}}_s)_{s=1}^{N_s}$, $\vec{\mathbf{x}}_s = (\varepsilon^2 \mathbf{x}_s, 0)$, is dense and that the source density (or cut-off profile) at the surface $z = 0$ is described by the function

$$\psi_s(\mathbf{y}_s) = \frac{N_s}{\pi b^2} \exp \left(- \frac{|\mathbf{y}_s|^2}{b^2} \right), \quad (45)$$

that is a Gaussian profile with radius b , so that we can use the continuum approximation (for any smooth test function ϕ)

$$\frac{1}{N_s} \sum_{s=1}^{N_s} \phi(\mathbf{x}_s) \simeq \frac{1}{\pi b^2} \int_{\mathbb{R}^2} \phi(\mathbf{y}_s) \exp \left(- \frac{|\mathbf{y}_s|^2}{b^2} \right) d\mathbf{y}_s.$$

The result stated in Proposition 3.3 is qualitatively true for an arbitrary form of the function ψ_s , but then the effective truncation function ψ_{eff} has no closed-form expression.

The finite aperture of the source array limits the angular diversity of the illumination, and as a result only a portion of the receiver array contributes to the cross correlation as characterized by the effective truncation function $\psi_{\text{eff}}(\mathbf{x}_q, \mathbf{y})$. In a homogeneous medium (left picture, figure 3) the effective truncation function has a clear geometric interpretation: only the receivers localized along rays going from the sources to the reflector can contribute. In a random medium, the angular diversity of the illumination is enhanced by scattering and

the effective truncation function is characterized by the effective source array diameter $\varepsilon^2 b_{\text{eff}}$ that depends on the source array diameter $\varepsilon^2 b$ and on the angular diversity enhancement induced by scattering (see (16)). Eq. (44) shows that, in terms of the effective receiver array diameter $\varepsilon^2 a_{\text{eff}}$ defined by (17), we have the following:

- If $a_{\text{eff}} > a$ so that $|\mathbf{x}_q - \mathbf{y}L/L_y| < a_{\text{eff}}$ for all $\vec{\mathbf{x}}_q = (\varepsilon^2 \mathbf{x}_q, L)$ in the receiver array, then the effective truncation function ψ_{eff} plays no role and we obtain the same result as in the case of a source array with full, infinite, aperture. The Kirchhoff migration function takes the form (51) below, in this case.
- If $a_{\text{eff}} < a$, then the effective truncation function ψ_{eff} does play a role and we obtain a result that is different from the case of a source array with full aperture. The Kirchhoff migration function takes the form (52) below, in this case.
- In both cases scattering is helpful as it increases the angular diversity and reduces the impact of the effective truncation function ψ_{eff} .

3.4 Kirchhoff Migration of Cross Correlations

The Kirchhoff migration function for the search point $\vec{\mathbf{y}}^S$ is

$$\mathcal{I}_C^\varepsilon(\vec{\mathbf{y}}^S) = \frac{1}{N_q^2} \sum_{q, q'=1}^{N_q} C^\varepsilon \left(\frac{|\vec{\mathbf{x}}_q - \vec{\mathbf{y}}^S| + |\vec{\mathbf{y}}^S - \vec{\mathbf{x}}_{q'}|}{c_0}, \vec{\mathbf{x}}_q, \vec{\mathbf{x}}_{q'} \right), \quad (46)$$

where N_q is the number of receivers at the auxiliary receiver array. The following proposition describes the resolution properties of the imaging function when the source array has full aperture. It is proved in [20].

Proposition 3.4 *If the auxiliary receiver array at the plane $z = L$ is a dense square array centered at $(\mathbf{0}, L)$ and with sidelength $\varepsilon^2 a$, if the source array covers the surface $z = 0$, if we assume additionally Hypothesis (47):*

$$\begin{aligned} & \text{The bandwidth } B \text{ of the source pulse is small compared} \\ & \text{to the central frequency } \omega_0, \end{aligned} \quad (47)$$

then, parameterizing the search point around the reflector by

$$\vec{\mathbf{y}}^S = \vec{\mathbf{y}} + (\varepsilon^2 \boldsymbol{\xi}, \varepsilon^4 \eta), \quad (48)$$

we have

$$\begin{aligned} \varepsilon^4 \mathcal{I}_C^\varepsilon(\vec{\mathbf{y}}^S) & \xrightarrow{\varepsilon \rightarrow 0} \frac{\sigma_{\text{ref}}}{64\pi^4 c_0 (L_y - L)^2 b^2} \text{sinc}^2 \left(\frac{\pi a \xi_1}{\lambda_0 (L_y - L)} \right) \text{sinc}^2 \left(\frac{\pi a \xi_2}{\lambda_0 (L_y - L)} \right) \\ & \times \exp \left(-i \frac{\omega_0}{c_0 (L_y - L)} (|\boldsymbol{\xi}|^2 + 2\boldsymbol{\xi} \cdot \mathbf{y}) \right) \int_{\mathbb{R}} i\omega |\hat{f}(\omega)|^2 \exp \left(2i \frac{\omega}{c_0} \eta \right) d\omega. \end{aligned} \quad (49)$$

This shows that the migration of the cross correlation gives the same result as if we were migrating the array response matrix of the auxiliary receiver array.

Indeed the imaging function (49) is exactly the imaging function that we would obtain if the medium was homogeneous, if the passive receiver array could be used as an active array, and if the response matrix of the array was migrated to the search point $\vec{\mathbf{y}}^S$. In particular the cross range resolution is $\lambda_0(L_y - L)/a$ (as given by the two sinc^2 functions in (49)) and the range resolution is c_0/B (as given by the integral in $|\widehat{f}(\omega)|^2$ in (49)).

The following proposition describes the resolution properties of the imaging function when the source array has finite aperture. It is proved in [21].

Proposition 3.5 *If the auxiliary receiver array at the plane $z = L$ is a dense square array centered at $(\mathbf{0}, L)$ and with sidelength $\varepsilon^2 a$, if the source array has finite aperture with diameter $\varepsilon^2 b$ and density (45), if we assume additionally Hypothesis (47), then, parameterizing the search point by (48) we have*

$$\begin{aligned} \varepsilon^4 \mathcal{I}_C^\varepsilon(\vec{\mathbf{y}}^S) &\xrightarrow{\varepsilon \rightarrow 0} \frac{\sigma_{\text{ref}}}{64\pi^4 c_0 (L_y - L)^2 b_{\text{eff}}^2} \text{sinc}\left(\frac{\pi a \xi_1}{\lambda_0 (L_y - L)}\right) \text{sinc}\left(\frac{\pi a \xi_2}{\lambda_0 (L_y - L)}\right) \\ &\times \frac{1}{a^2} \int_{[-a/2, a/2]^2} d\mathbf{x}_q \exp\left(-\frac{|\mathbf{x}_q - \mathbf{y}L/L_y|^2}{a_{\text{eff}}^2} + i \frac{\omega_0}{c_0 (L_y - L)} \boldsymbol{\xi} \cdot \mathbf{x}_q\right) \\ &\times \exp\left(-i \frac{\omega_0}{c_0 (L_y - L)} (|\boldsymbol{\xi}|^2 + 2\boldsymbol{\xi} \cdot \mathbf{y})\right) \int_{\mathbb{R}} i\omega |\widehat{f}(\omega)|^2 \exp\left(2i \frac{\omega}{c_0} \eta\right) d\omega. \quad (50) \end{aligned}$$

This shows that:

1. If the effective source array diameter is large enough so that $|\mathbf{x}_q - \mathbf{y}L/L_y| \leq a_{\text{eff}}$ for all $\mathbf{x}_q \in [-a/2, a/2]^2$, then we get the same result (49) as in the case of a source array with full aperture:

$$\begin{aligned} \varepsilon^4 \mathcal{I}_C^\varepsilon(\vec{\mathbf{y}}^S) &\xrightarrow{\varepsilon \rightarrow 0} \frac{\sigma_{\text{ref}}}{64\pi^4 c_0 L_y^2 a_{\text{eff}}^2} \text{sinc}^2\left(\frac{\pi a \xi_1}{\lambda_0 (L_y - L)}\right) \text{sinc}^2\left(\frac{\pi a \xi_2}{\lambda_0 (L_y - L)}\right) \\ &\times \exp\left(-i \frac{\omega_0}{c_0 (L_y - L)} (|\boldsymbol{\xi}|^2 + 2\boldsymbol{\xi} \cdot \mathbf{y})\right) \int_{\mathbb{R}} i\omega |\widehat{f}(\omega)|^2 \exp\left(2i \frac{\omega}{c_0} \eta\right) d\omega. \quad (51) \end{aligned}$$

2. If the effective source array diameter a_{eff} is smaller than a , then we get

$$\begin{aligned} \varepsilon^4 \mathcal{I}_C^\varepsilon(\vec{\mathbf{y}}^S) &\xrightarrow{\varepsilon \rightarrow 0} \frac{\sigma_{\text{ref}}}{64\pi^3 c_0 L^2 a^2} \text{sinc}\left(\frac{\pi a \xi_1}{\lambda_0 (L_y - L)}\right) \text{sinc}\left(\frac{\pi a \xi_2}{\lambda_0 (L_y - L)}\right) \\ &\times \exp\left(-i \frac{\omega_0}{c_0 (L_y - L)} (|\boldsymbol{\xi}|^2 + (2 - \frac{L}{L_y}) \boldsymbol{\xi} \cdot \mathbf{y})\right) \int_{\mathbb{R}} i\omega |\widehat{f}(\omega)|^2 \exp\left(2i \frac{\omega}{c_0} \eta\right) d\omega. \quad (52) \end{aligned}$$

Note that the difference with (51) is that the sinc functions have no square. This shows that the cross-range resolution is reduced (compared to the case of a source array with full aperture) and the range resolution is not affected.

Acknowledgments

We thank the Institut des Hautes Études Scientifiques (IHÉS) for its hospitality while this work was completed.

References

- [1] A. Bakulin and R. Calvert, The virtual source method: Theory and case study, *Geophysics*, **71** (2006), pp. SII39-SII50.
- [2] C. Bardos, J. Garnier, and G. Papanicolaou, Identification of Green's functions singularities by cross correlation of noisy signals, *Inverse Problems*, **24** (2008), 015011.
- [3] N. Bleistein, J. K. Cohen, and J. W. Stockwell, *Mathematics of Multidimensional Seismic Imaging, Migration, and Inversion*, Springer, New York, 2001.
- [4] P. Blomgren, G. Papanicolaou, and H. Zhao, Super-resolution in time-reversal acoustics, *J. Acoust. Soc. Am.*, **111** (2002), pp. 230-248.
- [5] L. Borcea, J. Garnier, G. Papanicolaou, and C. Tsogka, Coherent interferometric imaging, time gating, and beamforming, *Inverse Problems*, **27** (2011), 065008.
- [6] L. Borcea, J. Garnier, G. Papanicolaou, and C. Tsogka, Enhanced statistical stability in coherent interferometric imaging, *Inverse Problems*, **27** (2011), 085004.
- [7] L. Borcea, F. Gonzalez del Cueto, G. Papanicolaou, and C. Tsogka, Filtering deterministic layering effects in imaging, *SIAM Multiscale Model. Simul.*, **7** (2009), pp. 1267-1301.
- [8] L. Borcea, G. Papanicolaou, and C. Tsogka, Interferometric array imaging in clutter, *Inverse Problems*, **21** (2005), pp. 1419-1460.
- [9] L. Borcea, G. Papanicolaou, and C. Tsogka, Adaptive interferometric imaging in clutter and optimal illumination, *Inverse Problems*, **22** (2006), pp. 1405-1436.
- [10] Y. Colin de Verdière, Semiclassical analysis and passive imaging, *Nonlinearity*, **22** (2009), pp. R45-R75.
- [11] M. de Hoop and K. Sølna, Estimating a Green's function from field-field correlations in a random medium, *SIAM J. Appl. Math.*, **69** (2009), pp. 909-932.
- [12] A. Derode, P. Roux, and M. Fink, Robust acoustic time reversal with high-order multiple scattering, *Phys. Rev. Lett.*, **75** (1995), pp. 4206-4209.
- [13] W. Elmore and M. Heald, *Physics of Waves*, Dover, New York, 1969.
- [14] J.-P. Fouque, J. Garnier, A. Nachbin, and K. Sølna, Time reversal refocusing for point source in randomly layered media, *Wave Motion*, **42** (2005), pp. 238-260.
- [15] J.-P. Fouque, J. Garnier, G. Papanicolaou, and K. Sølna, *Wave Propagation and Time Reversal in Randomly Layered Media*, Springer, New York, 2007.
- [16] J.-P. Fouque, J. Garnier, and K. Sølna, Time reversal super resolution in randomly layered media, *Wave Motion*, **43** (2006), pp. 646-666.
- [17] J. Garnier, Imaging in randomly layered media by cross-correlating noisy signals, *SIAM Multiscale Model. Simul.*, **4** (2005), pp. 610-640.
- [18] J. Garnier and G. Papanicolaou, Passive sensor imaging using cross correlations of noisy signals in a scattering medium, *SIAM J. Imaging Sci.*, **2** (2009), pp. 396-437.
- [19] J. Garnier and G. Papanicolaou, Resolution analysis for imaging with noise, *Inverse Problems*, **26** (2010), 074001.
- [20] J. Garnier and G. Papanicolaou, Correlation based virtual source imaging in strongly scattering media, *Inverse Problems*, **28** (2012), 075002.

- [21] J. Garnier and G. Papanicolaou, Role of scattering in virtual source array imaging, *SIAM J. Imaging Sci.*, **7** (2014), pp. 1210-1236.
- [22] J. Garnier, G. Papanicolaou, A. Semin, and C. Tsogka, Signal-to-noise ratio estimation in passive correlation-based imaging, *SIAM J. Imaging Sci.*, **6** (2013), pp. 1092-1110.
- [23] J. Garnier and K. Sølna, Coupled paraxial wave equations in random media in the white-noise regime, *Ann. Appl. Probab.*, **19** (2009), pp. 318-346.
- [24] A. Ishimaru, *Wave Propagation and Scattering in Random Media*, IEEE Press, Piscataway, 1997.
- [25] G. Papanicolaou, L. Ryzhik, and K. Sølna, Statistical stability in time reversal, *SIAM J. Appl. Math.*, **64** (2004), pp. 1133-1155.
- [26] G. Papanicolaou, L. Ryzhik, and K. Sølna, Self-averaging from lateral diversity in the Ito-Schrödinger equation, *SIAM Multiscale Model. Simul.*, **6** (2007), pp. 468-492.
- [27] G. T. Schuster, *Seismic Interferometry*, Cambridge University Press, Cambridge, 2009.
- [28] F. D. Tappert, The Parabolic Approximation Method, in *Wave Propagation and Underwater Acoustics*, Springer Lecture Notes in Physics, **70** (1977), pp. 224-287.
- [29] B. J. Uscinski, *The Elements of Wave Propagation in Random Media*, McGraw Hill, New York, 1977.
- [30] K. Wapenaar, E. Slob, R. Snieder, and A. Curtis, Tutorial on seismic interferometry: Part 2 - Underlying theory and new advances, *Geophysics*, **75** (2010), pp. 75A211-75A227.